Title

Characterizing interactions in E-cadherin assemblages

Journal

Biophysical Journal, 122(15)

ISSN

0006-3495

Authors

Shome, Sayane

Jia, Kejue

Sivasankar, Sanjeevi

et al.

Publication Date

2023-08-01

DOI

10.1016/j.bpj.2023.06.009

Peer reviewed

Biophysical Journal
Article

Biophysical Society

Characterizing interactions in E-cadherin assemblages

Sayane Shome,[1] Kejue Jia,[1] Sanjeevi Sivasankar,[2] and Robert L. Jernigan[1,*]
[1]Roy J. Carver Department of Biochemistry, Biophysics and Molecular Biology, Iowa State University, Ames, Iowa and [2]Department of Biomedical Engineering, University of California, Davis, Davis, California

ABSTRACT Cadherin intermolecular interactions are critical for cell-cell adhesion and play essential roles in tissue formation and the maintenance of tissue structures. In this study, we focus on E-cadherin, a classical cadherin that connects epithelial cells, to understand how they interact in *cis* and *trans* conformations when attached to the same cell or opposing cells. We employ coevolutionary sequence analysis and molecular dynamics simulations to confirm previously known interaction sites as well as to identify new interaction sites. The sequence coevolutionary results yield a surprising result indicating that there are no strongly favored intermolecular interaction sites, which is unusual and suggests that many interaction sites may be possible, with none being strongly preferred over others. By using molecular dynamics, we test the persistence of these interactions and how they facilitate adhesion. We build several types of cadherin assemblages, with different numbers and combinations of *cis* and *trans* interfaces to understand how these conformations act to facilitate adhesion. Our results suggest that, in addition to the established interaction sites on the EC1 and EC2 domains, an additional plausible *cis* interface at the EC3-EC5 domain exists. Furthermore, we identify specific mutations at *cis/trans* binding sites that impair adhesion within E-cadherin assemblages.

SIGNIFICANCE Cell-cell adhesion depends on interactions of different types between cadherins on the interacting cells. The intention of this study is to develop some understanding of how the different types of interactions affect adhesion by means of molecular dynamics simulations.

INTRODUCTION

Cadherins are a superfamily of cell-cell adhesion proteins that facilitate the formation and organization of complex tissue structures. When two cells contact one another, cadherins from the opposing cells form *trans* bonds across the contact. In addition to *trans* bonds, adhesion is strengthened by *cis* dimer formation via lateral interactions of cadherins on the same cell surface (1). Among the most widely studied cadherins is the classical E-cadherin (Ecad), which plays a key role for cell-cell adhesion in epithelial tissues. Ecads have been shown to be essential for the formation and maintenance of epithelial structures (2,3). They are localized on the surfaces of epithelial cells at cell-cell contacts known as *adherens* junctions (4).

The extracellular regions of Ecad have five extracellular (EC) domains with Ca^{2+} ions binding at the linkers between the EC domains. Previous studies suggested that Ecads bind in two distinct *trans* conformations: a strand-swap dimer, where a highly conserved W at position 2 (W2) is embedded in a hydrophobic cavity formed on the other cadherin and X-dimers where the cadherins interact by one EC1 domain interacting with an EC2 domain on the interacting Ecad in an entirely different way (5–11). Based on contacts observed in the x-ray crystal structures of Ecads, it was proposed that interactions between the EC1 and EC2 domains of neighboring Ecads mediate *cis* dimerization with interactions between residues L175 and V81 (12,13). Studies have suggested that *cis* dimerization of Ecads requires previous *trans* dimerization (1,14), whereas single-molecule studies showed that *cis* dimerization also enhances the likelihood of Ecad *trans* binding (15). Multiple *trans* and *cis* contacts yield clusters resembling 2D lattices (12).

Both *trans* and *cis* interactions are considered to be quite sensitive and relatively easily disrupted. Studies demonstrated that all forms—the two *trans* forms and the *cis* form—are

Submitted April 21, 2022, and accepted for publication June 14, 2023.

*Correspondence: jernigan@iastate.edu

Sayane Shome's present address is Department of Anesthesiology, Perioperative and Pain Medicine, Stanford University School of Medicine, Stanford University, Stanford, CA, USA

Editor: Yuji Sugita.

https://doi.org/10.1016/j.bpj.2023.06.009

broken by the introduction of single mutations at the *trans* and *cis* binding interfaces. The mutation W2A abolishes the *trans* strand-swap dimer and traps Ecad in the X-dimer conformation (13). Similarly, K14E prevents the *trans* X-dimer formation and traps Ecad in the strand-swap dimer form. Likewise, the mutation L175D prevents formation of *cis* dimers. These critical amino acids (W2, K14, and L175) are highly conserved residues across many cadherin sequences in different species and have been suggested to act as "pegs" that "lock" these three *trans* and *cis* binding interfaces together.

In the present study, we obtain new insights into how several specific intermolecular residue pairs form contacts, defining interfaces, how they behave in various Ecad assemblages, and how they contribute to adhesion. For this purpose, we have carried out a set of computational analyses as highlighted in the flowchart in Data S1. We focus on the Ecad assemblages comprised of five and two monomeric units of three-dimensional structures of mouse Ecad (PDB: 3Q2V). Furthermore, we carried out coevolution analysis of all cadherin sequences (as they are homologous in nature to Ecads) to find the set of amino acid residue pairs showing a higher degree of coevolution across the Ecad assemblages, suggesting that they form contacts. This helps us to identify some sets of coevolving residues, including the residue pair (P231 and A491) located in EC3 and EC5 of adjacent Ecad units. We further investigate how much stronger the interactions at this interface are in comparison with known *cis* and *trans* binding interfaces, particularly in the absence (from production molecular dynamics simulations) and in the presence of forces applied at the known *cis* interfaces (from steered MD [SMD] simulations). In addition, we carry out some computational mutagenesis studies to find the lethal set of mutations that can plausibly impact the Ecad assemblages and study their effects from our production molecular dynamics simulations.

MATERIALS AND METHODS

The crystal structure of Ecad used for creating assemblages of Ecads

The structure of mouse Ecad is obtained from the Protein Data Bank (PDB) (PDB: 3Q2V). The structure obtained from the PDB is processed to remove all heteroatoms except calcium ions and retain only protein atoms and calcium ions. In addition, protein assemblages of two and five units of Ecads are created by using the PDB structure file with the Pymol (33) Symmetry plugin.

Coevolution analysis of residues from Ecad assemblages

The amino acid types at specific positions in a protein family are correlated because of evolutionary constraints, and physical constraints within the structure (structural packing constraints). The correlated amino acid changes can be observed in the interdependent changes within multiple sequence alignments (MSAs), such as an interacting large-small pair of amino acids being exchanged for a small-large pair. These correlated positions have been identified by global statistical methods such as direct coupling analysis (DCA) that disentangle the direct and indirect correlations, with important successes in identifying amino acid contact pairs (17–19), protein-protein interaction predictions (20–23), and amino acid mutation assessments (24,25). The highly successful protein structure predictions from Deep Mind with AlphaFold2 (26) utilize the coevolution correlations to uncover hidden structural information from the huge volume of sequence data. The data source for coevolution methods are the MSAs of homologous sequences. The quality of an MSA significantly affects the performance of these coevolution methods for detecting these types of coevolution signals. In this project, we use DCA as implemented by Marks et al. to calculate the correlations between residue pairs from the MSAs of the cadherin family taken from the Pfam database (27). For data preparation, each sequence in the MSA is weighted by using sequence identities. This is a method developed to use all of the data, aiming to give greater weight to the more diverse data in the set, sometimes called redundancy weighting (28–30). The amino acid sequences are first clustered into groups with a cutoff value of 70% sequence identity. Within each group, any two sequences are at least 70% identical. Then each sequence in each group is weighted by a value of one over the number of sequences in the group. Finally, equal weights are given to each cluster, and all weights are normalized by dividing by the sum of all weights. The results for cadherins are shown in Fig. 1. The surprise there is that there are no strong contact pairs indicated, and in general there are only weak correlations among any of the pairs, except for those nearby in sequence, which are usually strong. There are, however, a few potential interactions sites that are identified in Table 1, which we investigate below.

Introducing mutations into the protein structures

Based on the coevolution analysis, we list those residues lying in the binding interfaces in Ecad-Ecad assemblages, which are apparently coevolving with critical amino acid residues K14, V81, and G85(12) (Figs. 1 and 2; Table 1, and Video S1). The distribution of DCA values resembles a skewed "bell" curve. We use a Z score-like measure (DCA value minus the global mean then divided by the standard deviation) to evaluate the significance of the coevolving signal. Positive Z scores for correlations indicate that residues are coevolving, further suggesting that these residue interactions are conserved throughout the evolution. Mutations in the coevolving positions for these critical residues can also significantly impact the interaction interface.

To understand how these specific residues interact, we carry out computational single-point mutagenesis. We calculate the impact of all 19 possible combinations of mutations at these residue sites using the Dynamut server (31), which predicts the extent of lethality of a mutation if introduced in a protein using the NMA (32) approach. Based on those values, we identify three mutations in Ecad-Ecad assemblage for production molecular dynamics (MD) studies. We introduce these mutants into the structures using Pymol (33) mutagenesis plugin.

Preparation, minimization, and equilibration of the systems for molecular dynamics simulations

A recent study (34) employed similar assemblages of 24 Ecad units to show that large assemblages of curved ectodomains are stabilized by *trans* and *cis* linkages, which they probed by applying SMD simulations (34). In our study, we have focused on smaller assemblages with a focus on the interaction changes at the *cis* and *trans* binding sites. To prepare the system for MD simulations (production MD and SMD), the protein has been solvated by considering the protein dimensions. Furthermore, we have added an appropriate number of Na^+ and Cl^- ions to maintain charge balance. These steps were performed using the VMD software (35). The next steps were carried out using the NAMD software (36). The system was minimized for 250,000 steps followed by equilibration initializing at 11 K. The equilibration is carried out with an increase of 1 K per time step until the system temperature reaches 310 K. The cutoff distance for local van der Waals and electrostatic interactions between atoms is taken as 12 Å and the pair list of distances as 14 Å. Periodic boundary

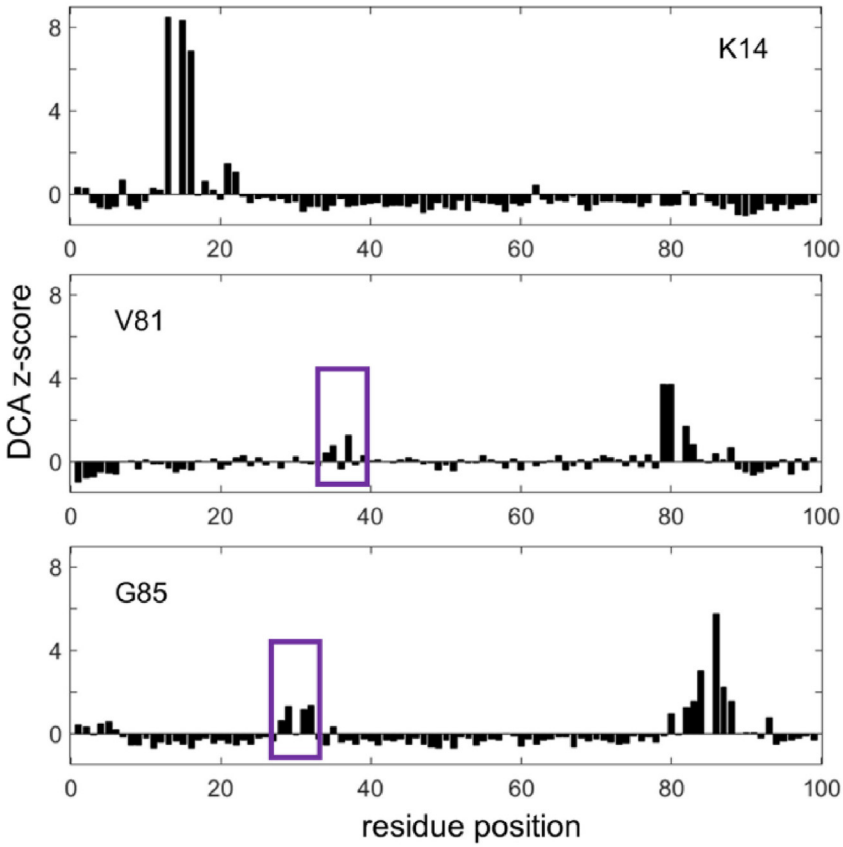

FIGURE 1 DCA *Z* scores of sequence correlations involving residues K14, V81, and G85. The sequence correlations for the entire protein are calculated using direct coupling analysis (DCA) (16,17) based on the multiple sequence alignments from the Pfam Database (PfamID: PF00028). The multiple sequence alignment contains 6,852 sequences. Each of the EC domains in cadherin corresponds to the same Pfam domain PF00028. Note that the residues have been reindexed to run from 1 to 100. The multiple sequence alignment (after removing gaps) has 100 positions The *Z* score is calculated using the raw DCA value minus the mean of all DCA values, then divided by the standard deviation. The highest *Z* scores indicate all three residues are strongly correlated with their sequence neighbors. Correlations with sequence-distant residues are relatively weak, but potentially defining of interactions, as identified by purple boxes and the specific residues are named in Table 1 also. The larger sequence-distant correlation values are listed in Table 1. Furthermore, all the mapped residues have been included in Data S4 and S5. To see this figure in color, go online.

conditions are applied to the system via the particle mesh Ewald method with a grid spacing of 1 Å. The remaining default parameters for the CHARMM27 force field are applied. We added a harmonic constraint of 1 kcal/mol Å^2 to some of the residues in EC4/EC5 units of the Ecad assemblage to mimic membrane anchorage in all the simulations. Production MD simulations are run for Ecad assemblages of 5 units for 15 ns with three replicates. For the SMD simulations, we apply a pulling force in $\pm x$, $\pm y$, $\pm z$ directions (six different directions) on the C^{α} atom of residues in the Ecad assemblages of 2 units at the *cis* interface (L175 and V81) with a constant velocity of 140 Å/ns and a force constant of 10 kcal mol^{-1} Å^2. We carried out 10 replicates for each case of SMD pulling direction, resulting in 60 independent simulations. MD trajectory data analyses (including dynamic cross correlation analysis) are performed using the VMD plugins (35) and Bio3d package in R (37). For studying the impact of single-point mutations on Ecad assemblages, production MD simulations are run on the Ecad assemblages of 2 units for 100 ns with 3 replicates.

RESULTS AND DISCUSSION

Identifying residues critical for adhesion in Ecad assemblages from a coevolutionary perspective

Coevolution methods based on the interpretation of evolutionary couplings have been proven to predict protein interactions (40–45). For instance, DCA has successfully predicted binary protein interactions in *Escherichia coli* (46). Here, we use DCA to evaluate the level of coevolution correlation for all pairs formed between two proteins to predict the interacting residues. With DCA analysis, we are able to derive all the residues from the query alignments that are coevolving. Previous studies confirmed that four residues W2, K14, V81, and L175 are primarily important for Ecad adhesion. We focus on finding if there are other residues in EC1-EC2 and EC3-EC5 regions that have a high degree of coevolution with these four residues particularly with L175. Our objective is to find out whether there are other residues that might cooperate with L175 to facilitate the cadherin *cis* interactions.

The MSA shows that residues W2 and L175 are conserved, which means that there are almost no mutations at these positions, and it should be noted that highly conserved residues cannot show correlations in sequence, since completely conserved invariant residues can only have a sequence correlation value of zero. This explains the low coevolution scores of residue pairs involving W2 and L175. K14 does not directly coevolve with L175 but it shows some coevolution signal with V174, which itself is correlated with L175. The overall coevolution signal of L175 is relatively weaker compared with other strongly coevolved positions due to its

TABLE 1 Correlated residues involving K14, V81, and G85 found in Ecad-Ecad assembly based on PDB: 3Q2V

Residue ID	Correlated residue IDs
K14	I7, L21, V22, V174 (62)
V81	V34, F35, S37, P65, I71, A491 (55)
G85	R28, D29, E31, T32, E93

Numbers in parentheses correspond to the residue indexes shown in Fig. 1.

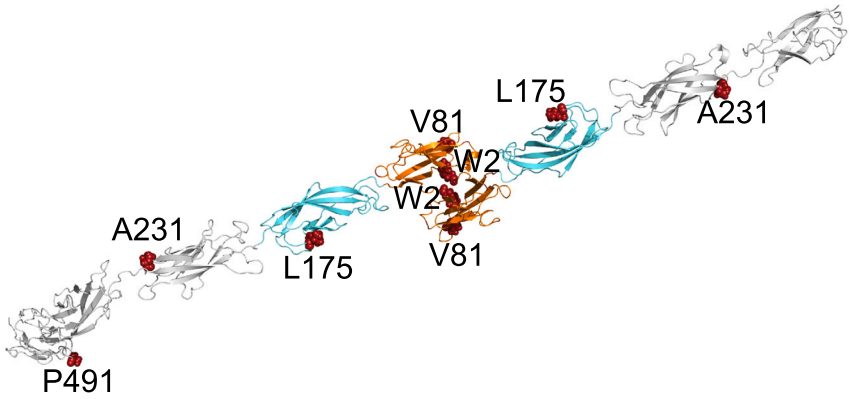

FIGURE 2 Structure of one Ecad ectodomain (PDB: 3Q2V (12)) *trans* dimer. This structure has been used for building the larger assemblages. The dark-red spheres identify the locations of the important featured residues—L175, W2, V81, P231, and A491. Here, EC1 domains are colored in orange and EC2 domains are cyan. To see this figure in color, go online.

high level of conservation. However, even a relatively weak coevolution value can be important if the residues are highly conserved since high levels of conservation naturally weaken the coevolution values. Therefore, we analyze the ranked residues showing the strongest coevolution signal for L175. Many residues show correlations with their close sequence neighbors, which are not viewed to be important since these are common, as can be seen in Fig. 1. Other residues including P231 and A491, which are the newly found interacting *cis* pair, also coevolve with L175. This residue pair is located within a distance of 5 Å of 175 on the neighboring Ecad unit. There is also some coevolution signal between A491 and V81. In Table 1, we list all the strongly correlated distant residues with K14, V81, and G85.

SMD applied to the interacting residues at the *trans* and *cis* binding sites in Ecad assemblages

In the current study, we employ computational simulations to understand the impact of different forces on *cis-cis* and *cis-trans* binding sites since these relate directly to cell adhesion.

Based on the structure PDB: 3Q2V (12), we have built Ecad assemblages having various numbers of *cis* and *trans* binding interfaces, as structures for performing MD simulations. The Ecad assemblage used in SMD simulations is comprised of two *trans* binding sites and one *cis* binding site (Fig. 3 *a*). Our aim is to investigate interactions at the *trans* and *cis* binding sites and also detect any localized conformational changes that can be observed at *cis-cis* and *cis-trans* binding sites when forces are applied in all three perpendicular directions in the system ($\pm x$, $\pm y$, $\pm z$) at the *cis* binding sites (C^{α} atoms of V81 and L175). We carried out 10 replicates for each case to make sure our observations are reliable (38). The goal of these SMD simulations is to investigate interaction and conformational changes, when Ecad assemblages are subjected to mechanical forces. Since these assemblages span opposing cells, and physiologically relevant mechanical forces are exerted by the underlying actomyosin cytoskeleton, we choose our force directions in the SMD simulations to mimic the physiological forces. The results suggest that W2 remains embedded in the binding cavity of residues from the neighboring Ecad units until the whole assemblage breaks down because of pulling at *cis* binding sites, as suggested by previous studies (12) (Videos S2 and S3). To quantify the MD simulations, we compute the interaction energies that are the total interaction energies in kcal/mol (36,39). In the MD simulations, the interaction energies between two residues i and j are evaluated as the sum of the non-bonded interaction energies defined by the force field (39). Nonbonded interaction energies that are considered include the van der Waals and electrostatic terms.

We observe nonzero favorable interaction energies between W2 residue and residues 89–92 in its hydrophobic binding cavity except in one case (where the *cis* interface is pulled in $+x$ direction), where at the end of the SMD simulation the *cis* interactions between EC1 and EC2 domains are broken (Fig. 3; Data S3).

Interestingly, we observe a novel *cis* interaction between residues 231 and 491 located in EC3 and EC5 of neighboring Ecad units, which has not been reported previously. This interaction is observed in all assemblages built by using crystallographic symmetry, after minimization. This approach to construct assemblages using the crystal lattice was utilized previously (12) to report the residues interacting at the *cis* binding sites in the Ecad units at EC1-EC2 domains. The connection between 231 and 491 between two neighboring Ecad units (observed after assemblage construction using crystal lattice) proved to be strong enough to sustain the linkage between these neighboring Ecad units, even when forces are applied on the *cis* (V81 and L175) interfaces in our SMD simulations (Fig. 3; Data S2).

Understanding the impact of protein dynamics in adhesion function of Ecad units

Furthermore, we carried out production MD simulations for different plausible Ecad assemblages to understand how these interfaces (*cis*, *trans*, and the newly discovered *cis* between EC3 and EC5 domains) sustain binding in the

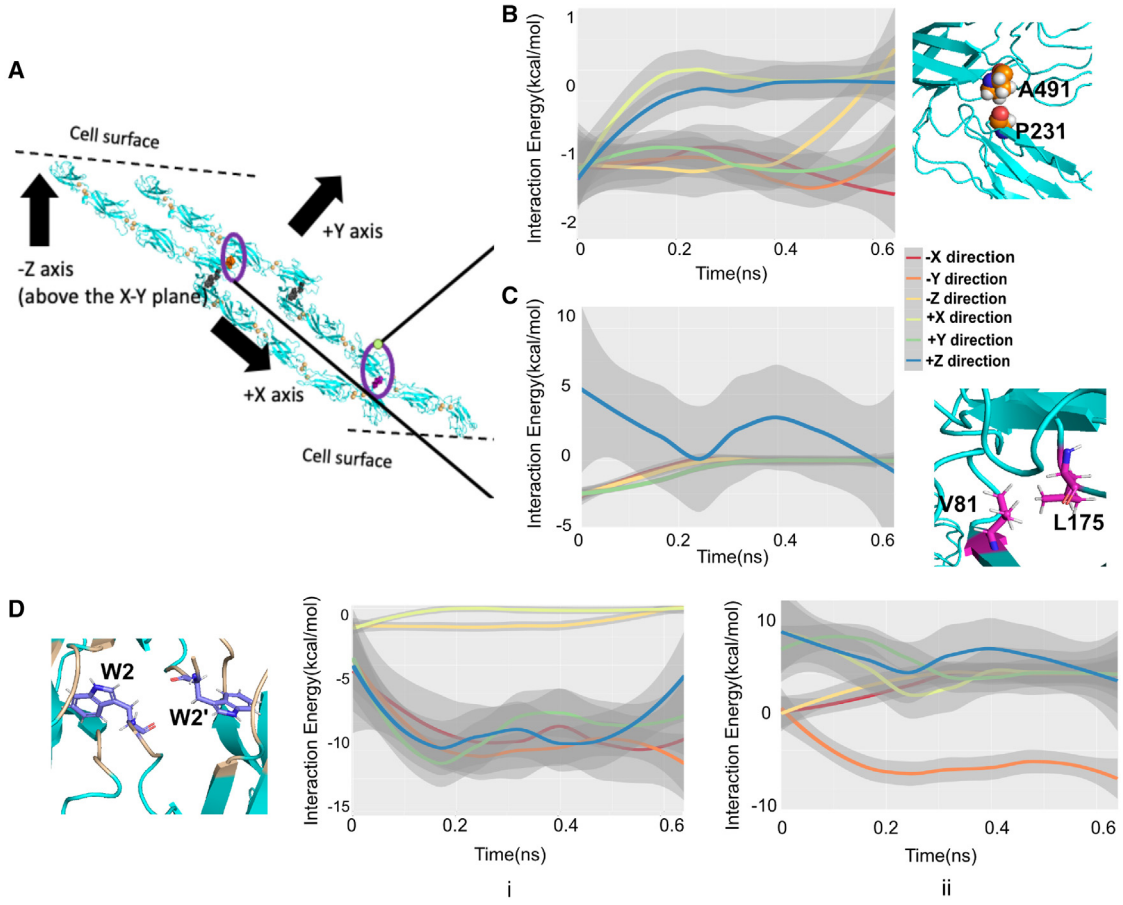

FIGURE 3 Steered MD simulations of four Ecad ectodomains interacting in *trans* and *cis* orientations, when the *cis* interface (V81 and L175) is pulled in different directions ($\pm x$ or $\pm y$ or $\pm z$). (*A*) The Ecad assemblage showing two *trans* interactions (*purple spheres*) and two *cis* interactions—one at EC1-EC2 (*pink spheres*), together with the newly discovered *cis* interaction between EC3 and EC5 (*orange spheres*). (*B*) Interaction energy profiles of the novel *cis* interface at EC3-EC5 (A491 and P231) and (*C*) Interaction energy profile of *cis* residues at EC1-EC2 (L175 and V81), respectively. At a *trans* interface, the W2 residues interact with neighboring hydrophobic cavities from the opposed Ecad ectodomain. (*D*) Here, we display the interaction energy profile of one of the W2/W2′ residues, embedded in the hydrophobic cavity; 1) interaction energy profile of W2 in hydrophobic cavity (residues 89 to 92), 2) interaction energy profile of W2′ in the hydrophobic cavity (residues 89–92). To see this figure in color, go online.

absence of any stress or force application in the larger assemblages of 5 units. Our results suggest that the interaction energy of the *cis* interaction between 231 in EC3 and 491 in EC5 is a weaker interaction compared with the *cis* interaction between the EC1 and EC2 domains (Figs. 4 *c* and *d*). Although, the *cis* interaction between 231 with 491 is weaker, it is observed throughout the simulations that include replicates (Fig. 4 *e*). In addition, our results suggest that the W2 *trans* dimerization is strong and interaction energies (Fig. 4 *b*) remain stable throughout the simulations of 15 ns duration. The interatomic distances between W2 and the hydrophobic cavity also remain fairly constant throughout these simulations (Fig. 5). Furthermore, to determine whether the residues at the *cis*/*trans* interfaces participate in long-distance coupling, we have carried out dynamic cross correlation analysis focusing particularly on amino acids W2, V81, L175, P231, and A491. Our results suggest the L175 and V81 display positive dynamic correlation with P231 and A491, meaning that these units move in similar directions during the MD simulation of 100 ns (Data S6). However, it should be noted that this is a preliminary result, which may need further validation.

Effects of single-point mutations on protein dynamics and the effect on adhesion

We introduce all possible 19 combinations of single-point mutations at G85, F35, and L175 in the Ecad-Ecad assemblage and utilize the Dynamut server to compute the impact of these mutations. Residues G85 and F35 were chosen because they are two of the amino acid residues facing L175 from the opposite side in the conserved *cis* interface reported previously in (12). Dynamut incorporates the ENCOM (47) and ANM models (48) to determine whether the introduction of a mutation would affect the protein properties based on entropy and energy calculations. Based on the extent of destabilizing scores obtained from the Dynamut results, we chose three mutations (G85D, L175G, and F35G)

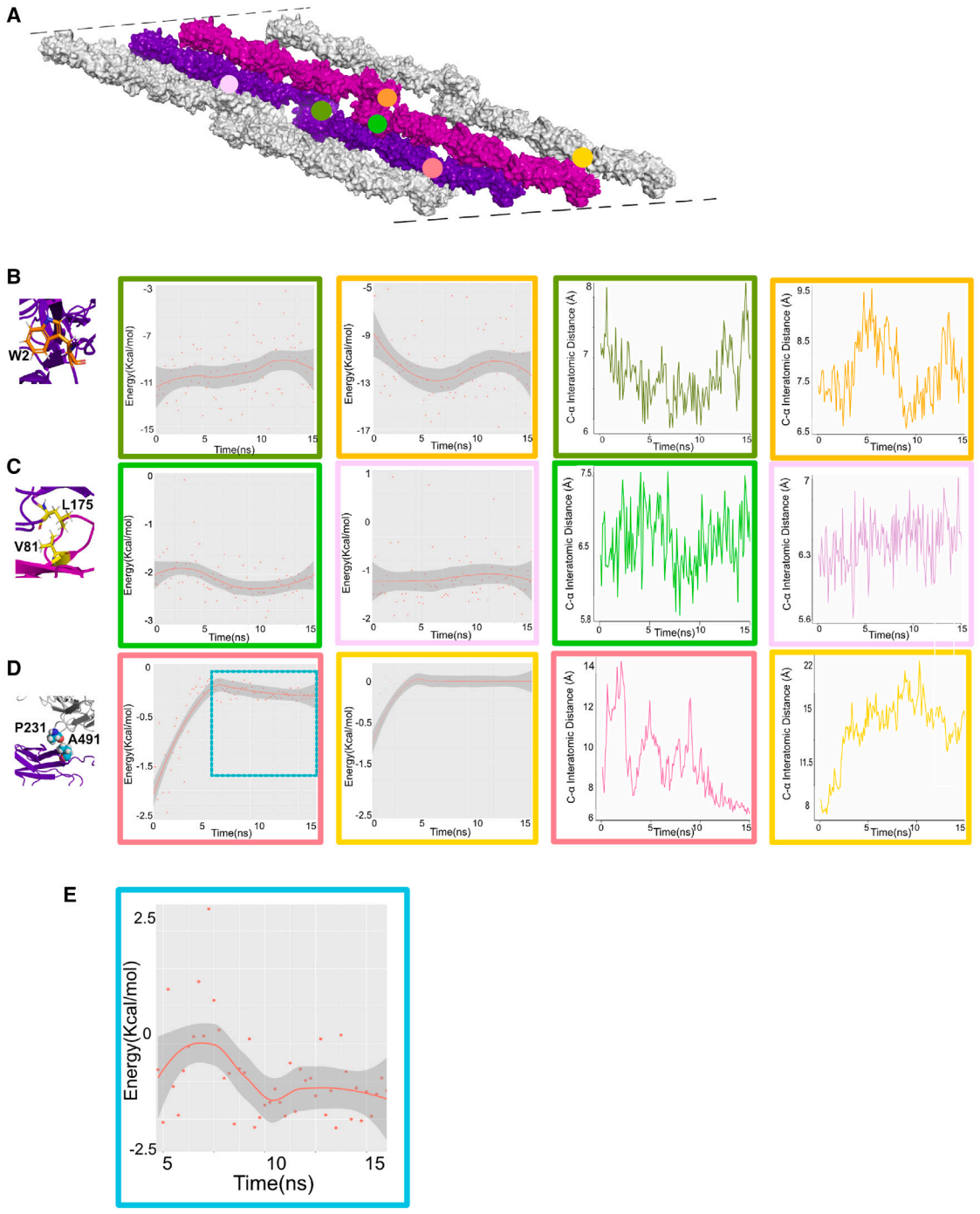

FIGURE 4 Protein dynamics in a large Ecad assemblage with five *trans* chains showing the role of interacting intermolecular residues during a production simulation of 15 ns. (*A*) There are five chains, comprised of ten separate cadherins in this assemblage (one chain is hidden below the plane in the present view). Results show how the interactions at the *cis* and *trans* interfaces change, particularly between the pink and purple central Ecad chains. To identify these, we have marked the specific interactions with colored dots: two *trans* interface pairs comprised of W2 and W2′ with dark green and orange dots; the usual *cis* interface at EC1-EC2 (L175 and V81) in mauve, purple, and bright green dots, respectively, and the new *cis* interface at EC3-EC5 (A231 and P491) marked with pink and yellow dots. (*B*) Interaction energies and C^{α} interatomic distances for one of the *trans* interfaces W2/W2′ with residues E89, M90, and D92 from the neighboring Ecad forming the hydrophobic cavity. (*C*) Interaction energies and C^{α} interatomic distances at the *cis* interaction between L175 and V81 (both pairs). (*D*) Interaction energies and C^{α} interatomic distances at the newly identified *cis* interaction between A231 and P491; we have highlighted the interaction energies between 5 and 15 ns with a blue box. (*E*) Interaction energy profile of the newly identified *cis* interaction between A231 and P491 between 5 and 15 ns suggests that, while interaction energies are weaker compared with the *cis* interaction between L175 and V81, they do persist throughout the simulation. To see this figure in color, go online.

Figure360▷ For a Figure360 author presentation of this figure, see https://doi.org/10.1016/j.bpj.2023.06.009.

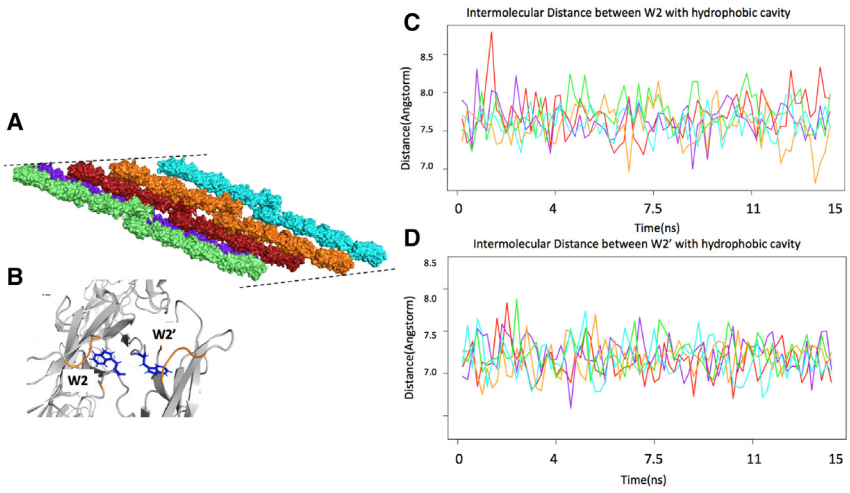

FIGURE 5 Intermolecular distances of all *trans* interaction sites (W2 and W2′ with their respective hydrophobic cavities) in Ecad assemblages of the same five units as in Fig. 3, during a production MD of 15 ns, shows that they do not vary much. (*A*) Each Ecad *trans* dimer is shown in different colors for the intermolecular distances between the W2/W2′ and the hydrophobic cavity where they are embedded. (*B*) Intermolecular distances between the C^{α} atom of W2 and center of mass of the hydrophobic cavity where it is buried in the *trans* binding sites in this Ecad assemblage. (*C*) Intermolecular distances between the C^{α} atom of W2 and the center of mass of the hydrophobic cavity where W2 is buried for all the *trans* interactions in the Ecad assemblage. (*D*) Intermolecular distances between the C^{α} atom of W2′ and the center of mass of the hydrophobic cavity where W2′ is buried for all the *trans* interactions in the Ecad assemblage. The two tryptophans (as observed in the previous figure as well) are in symmetric positions. Overall, this suggests that the strand-swapped dimer interactions are quite stable and do not change significantly overall during the simulations. To see this figure in color, go online.

for MD simulations. We introduce single-point mutations in the assemblages of 2 units and perform production MD simulations for 100 ns for each of the mutated assemblages and the native assemblage. Results suggest root mean-square fluctuations increase upon introducing these mutations into the assemblages (Fig. 6). The surprising result is that, in every case, the mutations appear to be substantially destabilizing the assemblage, as interpreted from the significantly larger fluctuations. These mutations will all significantly negatively impact binding. These observations, in general, show that computational screening can rapidly assess the effects of mutants upon the stability of cadherin assemblages.

CONCLUSIONS

Based on coevolution analysis, we were able to find residue pairs all across the EC domains, which are weakly coevolving across different species. It is a general principle that if two amino acids interact between proteins, these can be identified from sequence correlations because if they are close contact pairs then their sequences coevolve across those interfaces (49). Because they are close, then maintaining these interactions requires replacing the interacting pair in a coordinated way. Such coordinated amino acid compensations are frequently observed inside densely packed proteins. From our study, we learned of a new *cis* interaction between the EC3 and EC5 domains in Ecad assemblage, which is able to help support adhesion between neighboring Ecad units. Simulations of point mutations have provided insights into the importance of specific interacting amino acids in sustaining larger assemblages.

SUPPORTING MATERIAL

Supporting material can be found online at https://doi.org/10.1016/j.bpj.2023.06.009.

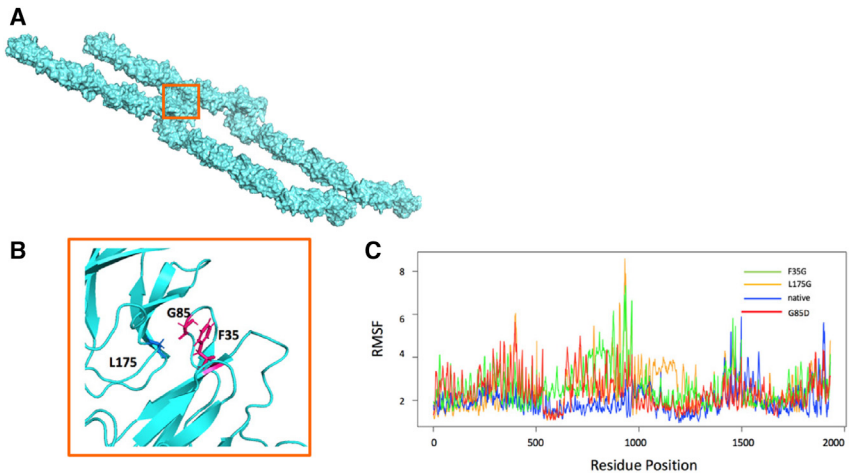

FIGURE 6 The effects of mutations at L175 and neighboring residues observed at a *cis* interface during production MD of 100 ns in the Ecad Assemblage of 2 units. (*A*) The Ecad assemblage of 2 chains; orange box is the part of the structure that is enlarged below. (*B*) G85 and F35 on neighboring Ecads is found to coevolve with L175 in the sequence data. (*C*) Production MD results suggest the root mean-square fluctuations increase significantly, throughout the structure, upon introduction of mutations on the Ecad assemblage. To see this figure in color, go online.

AUTHOR CONTRIBUTIONS

S. Sivasankar and R.L.J. developed the concepts, analyzed the data, and wrote the paper. S. Shome and K.J. performed the computations, analyzed the data, and wrote the paper.

ACKNOWLEDGMENTS

The authors gratefully acknowledge the support of grants NIH R01GM133880, NIH R01GM127701, NIH R01HG012117, and NSF PHY-1607550.

DECLARATION OF INTERESTS

The authors declare no competing interests.

REFERENCES

1. Wu, Y., X. Jin, …, A. Ben-Shaul. 2010. Cooperativity between Trans and Cis Interactions in Cadherin-Mediated Junction Formation. *Proc. Natl. Acad. Sci. USA.* 107:17592–17597.
2. Gloushankova, N. A., S. N. Rubtsova, and I. Y. Zhitnyak. 2017. Cadherin-mediated cell-cell interactions in normal and cancer cells. *Tissue Barriers.* 5, e1356900. https://doi.org/10.1080/21688370.2017.1356900.
3. Pereira, P. S., A. Teixeira, …, F. Casares. 2006. Cadherin missense mutations, associated with hereditary diffuse gastric cancer (HDGC) syndrome, display distinct invasive behaviors and genetic interactions with the Wnt and Notch pathways in Drosophila epithelia. *Hum. Mol. Genet.* 15:1704–1712. https://doi.org/10.1093/hmg/ddl093.
4. DeBeco, S., and C. Gueudry. 2020. Endocytosis Is Required for E-Cadherin Redistribution at Mature Adherens Junctions. *Proc. Natl. Acad. Sci. USA.* 117, 23191.
5. Sivasankar, S., Y. Zhang, …, S. Chu. 2009. Characterizing the initial encounter complex in cadherin adhesion. *Structure.* 17:1075–1081.
6. Bayas, M. V., A. Leung, …, D. Leckband. 2006. Lifetime measurements reveal kinetic differences between homophilic cadherin bonds. *Biophys. J.* 90:1385–1395. https://doi.org/10.1529/biophysj.105.069583.
7. Chien, Y. H., N. Jiang, …, D. Leckband. 2008. Two stage cadherin kinetics require multiple extracellular domains but not the cytoplasmic region. *J. Biol. Chem.* 283:1848–1856. https://doi.org/10.1074/jbc.M708044200.
8. Harrison, O. J., F. Bahna, …, L. Shapiro. 2010. Two-step adhesive binding by classical cadherins. *Nat. Struct. Mol. Biol.* 17:348–357. https://doi.org/10.1038/nsmb.1784.
9. Perret, E., A. Leung, …, E. Evans. 2004. Trans-bonded pairs of E-cadherin exhibit a remarkable hierarchy of mechanical strengths. *Proc. Natl. Acad. Sci. USA.* 101:16472–16477. https://doi.org/10.1073/pnas.0402085101.
10. Prakasam, A., Y. H. Chien, …, D. E. Leckband. 2006. Calcium site mutations in cadherin: impact on adhesion and evidence of cooperativity. *Biochemistry.* 45:6930–6939. https://doi.org/10.1021/bi060213m.
11. Shi, Q., V. Maruthamuthu, …, D. Leckband. 2010. Allosteric cross talk between cadherin extracellular domains. *Biophys. J.* 99:95–104. https://doi.org/10.1016/j.bpj.2010.03.062.
12. Harrison, O. J., X. Jin, …, B. Honig. 2011. The extracellular architecture of adherens junctions revealed by crystal structures of type I cadherins. *Structure.* 19:244–256. https://doi.org/10.1016/j.str.2010.11.016.
13. Shafraz, O., M. Rübsam, …, S. Sivasankar. 2018. E-cadherin binds to desmoglein to facilitate desmosome assembly. *Elife.* 7, e37629. https://doi.org/10.7554/eLife.37629.
14. Wu, Y., J. Vendome, …, B. Honig. 2011. Transforming binding affinities from three dimensions to two with application to cadherin clustering. *Nature.* 475:510–513. https://doi.org/10.1038/nature10183.
15. Zhang, Y., S. Sivasankar, …, S. Chu. 2009. Resolving cadherin interactions and binding cooperativity at the single-molecule level. *Proc. Natl. Acad. Sci. USA.* 106:109–114. https://doi.org/10.1073/pnas.0811350106.
16. Manibog, K., K. Sankar, …, S. Sivasankar. 2016. Molecular determinants of cadherin ideal bond formation: Conformation-dependent unbinding on a multidimensional landscape. *Proc. Natl. Acad. Sci. USA.* 113:E5711–E5720. https://doi.org/10.1073/pnas.1604012113.
17. Morcos, F., A. Pagnani, …, M. Weigt. 2011. Direct-coupling analysis of residue coevolution captures native contacts across many protein families. *Proc. Natl. Acad. Sci. USA.* 108:E1293–E1301. https://doi.org/10.1073/pnas.1111471108.
18. Marks, D. S., T. A. Hopf, and C. Sander. 2012. Protein structure prediction from sequence variation. *Nat. Biotechnol.* 30:1072–1080. https://doi.org/10.1038/nbt.2419.
19. Ovchinnikov, S., H. Kamisetty, and D. Baker. 2014. Robust and accurate prediction of residue–residue interactions across protein interfaces using evolutionary information. *Elife.* 3, e02030.
20. Cong, Q., I. Anishchenko, …, D. Baker. 2019. Protein interaction networks revealed by proteome coevolution. *Science.* 365:185–189. https://doi.org/10.1126/science.aaw6718.
21. Hopf, T. A., C. P. I. Schärfe, …, D. S. Marks. 2014. Sequence co-evolution gives 3D contacts and structures of protein complexes. *Elife.* 3, e03430. https://doi.org/10.7554/eLife.03430. PMC4360534.
22. Pokarowski, P., A. Kloczkowski, …, A. Kolinski. 2005. Inferring ideal amino acid interaction forms from statistical protein contact potentials. *Proteins.* 59:49–57. https://doi.org/10.1002/prot.20380. PMC4417612.
23. Muscat, M., G. Croce, …, M. Weigt. 2020. FilterDCA: Interpretable supervised contact prediction using inter-domain coevolution. *PLoS Comp Biol.* 16, e1007621. https://doi.org/10.1371/journal.pcbi.1007621.
24. Hopf, T. A., J. B. Ingraham, …, D. S. Marks. 2017. Mutation effects predicted from sequence co-variation. *Nat. Biotechnol.* 35:128–135. https://doi.org/10.1038/nbt.3769.
25. Figliuzzi, M., H. Jacquier, …, M. Weigt. 2016. Coevolutionary Landscape Inference and the Context-Dependence of Mutations in Beta-Lactamase TEM-1. *Mol. Biol. Evol.* 33:268–280. https://doi.org/10.1093/molbev/msv211.
26. Jumper, J., R. Evans, …, D. Hassabis. 2021. Highly accurate protein structure prediction with AlphaFold. *Nature.* 596:583–589. https://doi.org/10.1038/s41586-021-03819-2.
27. Bateman, A., L. Coin, …, S. R. Eddy. 2004. The Pfam protein families database. *Nucleic Acids Res.* 32:D138–D141.
28. Yanover, C., N. Vanetik, …, C. Keasar. 2014. Redundancy-weighting for better inference of protein structural features. *Bioinformatics.* 30:2295–2301.
29. Miyazawa, S., and R. L. Jernigan. 1996. Residue–residue potentials with a favorable contact pair term and an unfavorable high packing density term, for simulation and threading. *J. Mol. Biol.* 256:623–644.
30. Miyazawa S. , Jernigan R.L.. Self-consistent estimation of inter-residue protein contact energies based on an equilibrium mixture approximation of residues. Proteins, ,34:49-68.
31. Rodrigues, C. H., D. E. Pires, and D. B. Ascher. 2018. DynaMut: predicting the impact of mutations on protein conformation, flexibility and stability. *Nucleic Acids Res.* 46:W350–W355. https://doi.org/10.1093/nar/gky300.
32. Bahar, I., T. R. Lezon, …, I. H. Shrivastava. 2010. Normal mode analysis of biomolecular structures: functional mechanisms of membrane proteins. *Chem. Rev.* 110:1463–1497. https://doi.org/10.1021/cr900095e.
33. The PyMOL Molecular Graphics System, Version 1.2r3pre, Schrödinger, LLC.
34. Neel, B. L., C. R. Nisler, …, M. Sotomayor. 2022. Collective mechanical responses of cadherin-based adhesive junctions as predicted by simulations. *Biophys. J.* 121:991–1012.
35. Humphrey, W., A. Dalke, and K. Schulten. 1996. VMD - Visual Molecular Dynamics. *J. Mol. Graph.* 14:33–38.

36. Phillips, J. C., D. J. Hardy, …, E. Tajkhorshid. 2020. Scalable molecular dynamics on CPU and GPU architectures with NAMD. *J. Chem. Phys.* 153:044130. https://doi.org/10.1063/5.0014475.

37. Grant, B. J., A. P. C. Rodrigues, …, L. S. D. Caves. 2006 Nov 1. Bio3d: an R package for the comparative analysis of protein structures. *Bioinformatics.* 22:2695–2696. https://doi.org/10.1093/bioinformatics/btl461.

38. Phillips, J. C., R. Braun, …, K. Schulten. 2005. Scalable molecular dynamics with NAMD. *J. Comput. Chem.* 26:1781–1802. https://doi.org/10.1002/jcc.20289.

39. Serçinoglu, O., and P. Ozbek. 2018. gRINN: a tool for calculation of residue interaction energies and protein energy network analysis of molecular dynamics simulations. *Nucleic Acids Res.* 46:W554–W562. https://doi.org/10.1093/nar/gky381.

40. Weigt, M., R. A. White, …, T. Hwa. 2009. Identification of direct residue contacts in protein–protein interaction by message passing. *Proc. Natl. Acad. Sci. USA.* 106:67–72.

41. Marks, D. S., L. J. Colwell, …, C. Sander. 2011. Protein 3D structure computed from evolutionary sequence variation. *PLoS One.* 6, e28766.

42. Morcos, F., A. Pagnani, …, M. Weigt. 2011. Direct-coupling analysis of residue coevolution captures native contacts across many protein families. *Proc. Natl. Acad. Sci. USA.* 108:E1293–E1301. https://doi.org/10.1073/pnas.1111471108.

43. Ekeberg, M., C. Lövkvist, …, E. Aurell. 2013. Improved contact prediction in proteins: using pseudolikelihoods to infer Potts models. *Phys. Rev.* 87, 012707.

44. Kamisetty, H., S. Ovchinnikov, and D. Baker. 2013. Assessing the utility of coevolution-based residue-residue contact predictions in a sequence- and structure-rich era. *Proc. Natl. Acad. Sci. USA.* 110:15674–15679. https://doi.org/10.1073/pnas.1314045110.

45. Söding, J. 2017. Big-data approaches to protein structure prediction. *Science.* 355:248–249. https://doi.org/10.1126/science.aal4512.

46. Hopf, T. A., C. P. I. Schärfe, …, D. S. Marks. 2014. Sequence co-evolution gives 3D contacts and structures of protein complexes. *Elife.* 3, e03430. https://doi.org/10.7554/eLife.03430.

47. Frappier, V., and R. J. Najmanovich. 2014. A coarse-grained elastic network atom contact model and its use in the simulation of protein dynamics and the prediction of the effect of mutations. *PLoS Comput. Biol.* 10, e1003569. https://doi.org/10.1371/journal.pcbi.1003569.

48. Eyal, E., G. Lum, and I. Bahar. 2015. The anisotropic network model web server at 2015 (ANM 2.0). *Bioinformatics.* 31:1487–1489.

49. Cong, Q., I. Anishchenko, …, D. Baker. 2019. Protein interaction networks revealed by proteome coevolution. *Science.* 365:185–189. https://doi.org/10.1126/science.aaw6718.